

Investigating the Effect of Air Volume Fraction on the Velocity Distributions of Air-Water flow in a Pipe Separator

Eyitayo A. Afolabi¹ and J.G.M Lee²

¹Department of Chemical Engineering, Federal University of Technology, Minna, Nigeria.

²School of Chemical Engineering and Advanced Materials, Newcastle University, Newcastle upon Tyne, UK.

elizamos2001@yahoo.com

Abstract- A stereoscopic particle image velocimetry velocity field measurement technique was used to investigate the effect of air volume fraction on the velocity distribution of air-water flow in a pipe separator. The experiment was performed in a 30 mm ID three phase pipe separator at room temperature and atmospheric outlet pressure with air and water used as test fluids. Velocity distributions of air-water flow are measured at three different axial positions for six different air volume fractions. The experimental results revealed that the flow patterns of the tangential velocity and radial velocity are unaffected by the changes in the air volume fraction. However, their magnitudes are observed to be inversely proportional to air volume fraction. The effect of air volume fraction is mostly observed at the axial velocity profile at Z= 295 mm, where an increase in air volume fraction leads to more surface area occupied by the separated air.

Keywords: Stereoscopic particle image velocimetry; Hydrodynamics; Separations; Pipe separator

I. INTRODUCTION

The evolution of laser diagnostics has played an important role in making detailed and accurate experimental measurements possible. The PIV is non-intrusive measurement technique, causing no interference to the flow fields under investigation with the capability of obtaining measurements at extreme conditions. It also has the advantages of fast dynamic response, high spatial resolution and whole field measurement technique. As in [1] – [3], an excellent references for the history and up-to-date development of the PIV technique and its applications are well documented. Pitot-static tubes and miniature hot wire anemometry techniques suffer from inaccuracies when dealing with unsteady flow (such as the one observed in a separator), since the probe can intrude into the flow itself which possibly leads to deterioration. In addition, the Laser Doppler Velocimetry technique is a point based method and cannot simultaneously provide a three-dimensional velocity field associated with the swirl flow in the pipe separator. Stereoscopic particle image velocimetry (SPIV) is an extension of conventional 2-D PIV for

measuring the third velocity component in the laser light sheet plane [4].

In its simplest form, SPIV measurements involves the output of a pulsed or chopped high energy laser directed through a cylindrical and spherical lens system in order to shape the resulting beam into a thin planar light sheet. This sheet of light is subsequently aligned and directed to the flow of interest seeded with neutral density light scattering particles or dispersed air bubbles also known as tracer particles [5]. The incident planar light sheet then scatters to the viewing plane where images of the scattering seeds (bubbles or micron-sized particles) may be captured by a synchronized high-speed camera [6, 7]. A subsequent laser pulse is emitted at a short time interval relative to the flow velocity and then after the flow images of tracer particles are again captured at their new locations corresponding to the flow field. The resulting doubly exposed flow images represent the locations of the tracer particles following the flow at two discrete instances in time. The analysis of the resulting images requires measurement of the separation distance between successive flow images such that when combined with the known temporal separation, the desired velocity vectors may be determined [1]. The 2-D vector fields are then combined to give 3-D vector fields [4].

The PIV technique has been successfully used to obtain measurements of single phase flow velocity fields [8], and it can be extended to multiphase flows in order to obtain full field velocity measurements for each phase. Simultaneous measurements of the continuous and dispersed phases are extremely important in order to understand inter-phase interaction, and the concentrations, sizes and shapes of the dispersed phases. When the conventional PIV system is used for the measurement of a multiphase flow such as a bubbly flow, the intensity of light reflected from the surfaces of bubbles not only saturates the CCD camera but also overwhelms the intensity of light refracted from the seeding particles for

PIV in its vicinity [9]. The continuous phase can be differentiated from the dispersed phase by using fluorescent dyes and optical band pass filters. For example, the combination of the PIV technique with laser induced fluorescence (LIF) and/or the shadow image technique (SIT) are options available to measure the velocity distributions of the phases and their interaction [10]. However, PIV measurement techniques are limited to relatively low volume fractions (usually $\alpha \leq 5\%$) of the dispersed phase [11, 12]. As in [11] – [12], PIV was utilized to obtain a full-field quantitative description of a three-dimensional, two-phase bubbly flow in a rectangular vessel. They used the velocity information obtained by the PIV system to investigate the turbulence structure and the influence of bubbles on the surrounding flow field (bubble/flow interaction). PIV technique have been applied to measure the instantaneous full-field properties of the velocity components in gas–liquid–solid fluidization system as in [5] and to investigate gas–liquid flows in horizontal and slightly inclined pipes [13].

Compact separators are widely used as an effective and economical alternative to conventional separators which are expensive, heavy and bulky in size especially in offshore platforms in oil and gas production operations. They are simpler to operate, more lightweight, have neither moving nor internal parts, require less floor space, and involve lower capital and operational costs [14]. A pipe separator is a device used to separate dispersed phase(s) from continuous phase according to their density difference and size by centrifugal force. The three phase pipe separator has potential application as a free water knockout system in equipment for the upstream oil and gas production such as in down-hole, surface (onshore and offshore) and subsea separation [15]. The objective of this work is to carry out a detailed experimental investigation of the effect of air volume fraction on the tangential, axial, and radial velocities of air-water flow in a pipe separator using stereo-PIV. The knowledge gained from this investigation would make it possible to effectively select suitable range of air volume fraction necessary for optimum phase separation of multiphase flow in a pipe separator.

II. EXPERIMENTAL FACILITY AND PROCEDURE

Experimental Facility

A 30 mm ID laboratory prototype pipe separator based on one of the geometries developed for multiphase flow separation by the Separation Technology Project of the University of Tulsa, USA was fabricated and installed in the School of Chemical Engineering and Advanced Materials, Newcastle University, UK [16-17]. All experiments are conducted using water (density 996 kgm^{-3} , viscosity 0.001 kg/ms) and air (density 1.225 kgm^{-3} , viscosity 0.000018 kg/ms) at room temperature and

atmospheric outlet pressure. Water and air are pumped from their respective storage tanks, metered and introduced to the pipe separator via an inline mixer, which ensures minimum mixing. A detailed sketch of the separator test section is shown in Figure 1. The test section was constructed using a transparent perspex tube and the main body is a 30 mm ID vertical cylinder with a height of 1675 mm. The inlet is a 30-mm ID pipe, inclined at an angle of 27 degrees from the horizontal and connected tangentially at 585 mm from the top of the vertical main body. The inlet configuration was constructed by inserting a gradually reduced inlet nozzle designed by narrowing the inlet down from a full bore cross sectional area to 25% of the inlet cross sectional area. The flow from the three outlets was controlled using natural rubber bungs to specify the split ratio as a function of mass flow rate passing through each outlet.

Separation Mechanism

The air-water mixture enters the pipe separator through the inclined inlet designed to promote the pre-separation of the gas-liquid mixture. The tangential inlet with reduced area produces a swirling motion in the vertical cylindrical pipe. Due to the differences in density, the centrifugal effect segregates the air-water mixture, thereby allows air to flow upward and leaves through the gas outlet. In addition, water flow to the lower section of the pipe separator and flow out through the water and oil-rich outlets.

Air-Water flow Experiment

As a result of the nozzle inserted at the inlet junction of the pipe separator, the swirling motion of the segregated flow changes to different flow patterns away from the inlet section. During regular operation, a bubble, slug, churn or annular flow pattern is established inside the main body of the pipe separator [18]. As in [15], it was observed that cylindrical cyclone achieves more efficient separation with stratified flow pattern at the inclined inlet. Therefore, this investigation considered stratified wavy flow pattern of air-water mixture at the inclined inlet of the pipe separator.

At atmospheric pressure and room temperature, a stratified wavy flow pattern at the inlet section of the separator was observed with air flow rate of $0.000045 \text{ m}^3/\text{s}$. This air flow rate and corresponding water flow rates shown in Table 1 with their associated properties such as densities, viscosities and were then used to calculate and plot the Martinelli (X), and Taitel and Dukler (K) parameters onto the air-water flow map for inclined pipe [19- 20]. These parameters were observed to lie in the stratified wavy region and confirmed a segregated flow pattern occurring at the inlet section of the pipe separator.

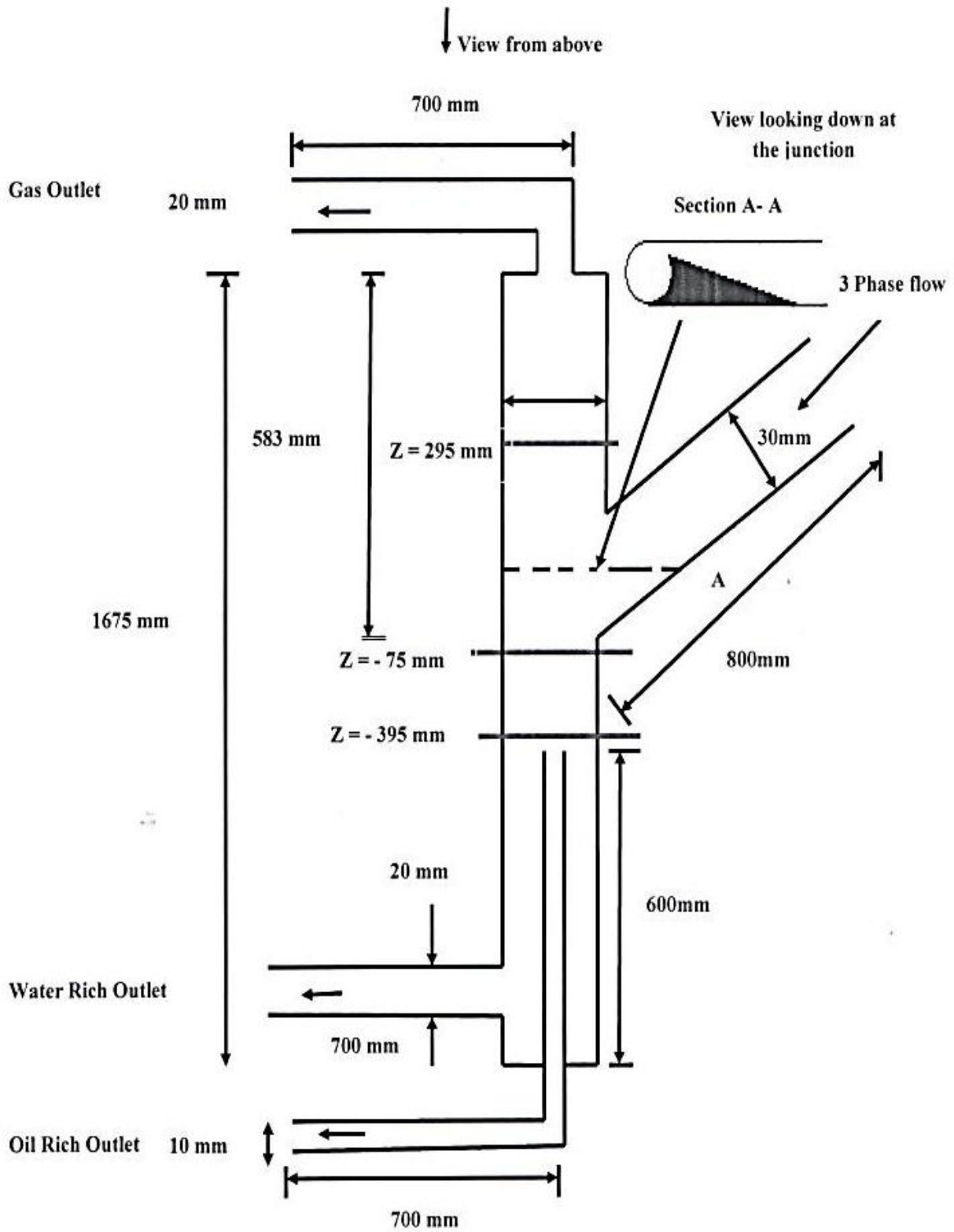


Figure 1. Three-Phase Pipe Separator System [15].

Table 1: Experimental runs for Air-Water Measurements.

	Gas flow rate (10 ⁻⁵ m ³ /s)	Water flow rate (10 ⁻⁴ m ³ /s)	Gas volume fraction (%)	Split ratio (water outlet)	Split ratio (air outlet)	Split ratio (oil outlet)
A	4.5	2.05	18.0	0.317	0.066	0.617
B	4.5	1.96	18.67	0.332	0.069	0.599
C	4.5	1.85	19.57	0.352	0.072	0.576
D	4.5	1.58	22.17	0.40	0.1	0.5
E	4.5	1.48	23.32	0.439	0.1	0.47
F	4.5	1.32	25.42	0.48	0.11	0.41

$$X = \sqrt{\frac{(\Delta P/L)L}{(\Delta P/G)G}} \quad (1)$$

$$K = \frac{U_G^2}{dg \cos \alpha} \left(\frac{\rho_G}{\rho_G - \rho_L} \right) \left(\frac{\rho_L d U_L}{\mu_L} \right) \quad (2)$$

In order to study the effect of air volume fraction on the velocity distributions of air-water flow in a pipe separator, experimental runs are carried out with constant air volumetric flow rate of 0.000045 m³/s and six different water flow rates as shown in Table 1. In addition, the split ratio for the water rich outlet is defined as the ratio of liquid flow rate passing through the water-rich outlet to the total liquid flow rate at the inlet.

Stereoscopic Particle Image Velocimetry (SPIV) set-up

The stereo-PIV system used for this investigation was manufactured by TSI Inc and loaned from the EPSRC engineering instruments pool. The SPIV set-up consist of a high repetition pulsed laser and a pair of high-speed cameras (Figure 3). The laser was a CFR-200 double pulsed Nd: YAG laser system designed by Big Sky Laser (USA), which has a capability of emitting a nanosecond pulse with a wavelength of 532 nm and energy of 200 mJ per pulse laser. A thin laser light sheet of 1 mm thickness was obtained using cylindrical and spherical lenses and pass through the laser beam through a TSI Model 610015 light arm to illuminate the plane of interest[17].

Two TSI Model 630059 POWERVIEW TM equipped with 4MP PIV cameras with CCD sensors are installed on the Scheimpflug mounts in order to satisfy the stereoscopic camera condition. The two cameras set at angle of +45° and - 45° to the light sheet by tilting the image sensor plane and the lens plane to the Scheimpflug condition, the plane best of focus could be found so that it aligned with the light sheet [4]. These cameras were positioned at both

sides of the light sheet 300 mm away from the measuring plane and then connected to a 64 bit frame grabber to capture and digitize images and communicate with a computer. A TSI 610035 laser pulse synchronizer was used to synchronize the laser and cameras.

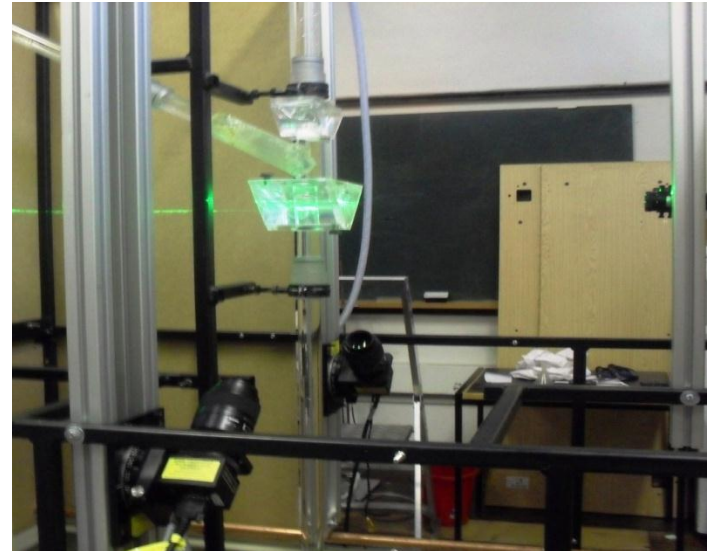


Figure 2: S-PIV experimental set-up

A water prism of 45 degrees was constructed and fitted to the frame supporting the experimental rig so as to align the cameras with the laser beam. The prism is then moved to the test section of the experimental rig in order to minimize optical distortion arising from refraction through the perspex wall. Seeding particles were 10070-3 fluorescent microsphere tracer particles (from TSI Inc.) capable of absorbing light of wavelength 532 nm and emitting it at 542 nm, so that the light reflected from the tracer particles could be used to measure the velocity field of the flow under investigation. An optical filter (long wavelength passes filter) was fitted to the cameras in order to prevent the reflection of scattered light from the gas bubbles.

Camera Calibration

A single-image camera calibration was performed using a calibration target populated by a cartesian grid of 2 mm white marker dots with a 3 mm cross at the centre on a black background. The cut to size calibration target was mounted on a flat plate and inserted into the test section to coincide exactly with the light sheet, and then after moved using a micrometer in seven steps of 0.5 mm (Z=-1.5,-1,-0.5, 0, 0.5, 1, 1.5 mm). The error in the movement of the micrometer was found to be less than 0.01 mm. At each measurement plane, the stereo-cameras were set to satisfy the Scheimpflug condition and images of the target were recorded and analysed by the perspective calibration method of the INSIGHT 3G software. The analysis of the calibration image produced a calibration mapping function that was used to combine 2-D PIV vector fields to a three-dimensional vector field.

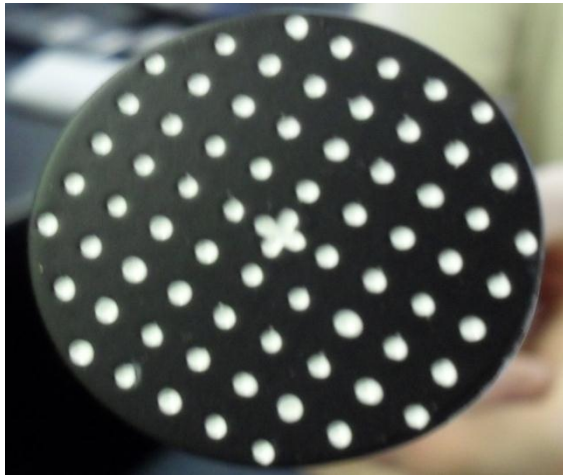


Figure 3: Calibration Target

SPIV Evaluation and Post-processing

A pair of two hundred images was recorded for water-air multiphase flow at three different axial positions $Z= -395$ mm, -75 mm and 295 mm along the vertical axis of the cyclone (Figure 1). The software INSIGHT 3G from TSI Inc was used to evaluate the recorded images via cross-correlation and the particle image subdivided into small interrogation windows. For each interrogation window the average particle image separation is determined by cross-correlation and localization of the correlation peak. In this work, a multi-pass processing scheme was used; consisting of two passes with interrogation windows of 64×64 pixels and 50% overlap. Another pass was applied with an interrogation area of 32×32 pixels and 50% overlap. Erroneous vectors were removed and replaced by a global velocity filter and local 3×3 median filters. The outliers were finally interpolated to fill gaps in the vector fields. Dividing with the known time between the two images captured the displacement vectors are converted into velocity vectors as follows:

$$\bar{w} = \frac{\Delta \bar{x}}{\Delta t} \quad (3)$$

where \bar{w} is the velocity vector, \bar{x} is the average displacement vector and \bar{t} denotes the time delay between two image frames. A pair of velocity vectors obtained from the left and right cameras was combined to reconstruct three-component velocity vectors using the calibration mapping function obtained from the analysis of the camera calibration as described earlier. However, it is impossible to measure the velocity distribution of each of the phases due to the high volume fraction of air. Therefore, the conventional SPIV image processing technique was applied to the air-water flow velocity maps which cannot separate between the velocity distributions of each phase present in the air-water multiphase flow.

III. RESULTS AND DISCUSSION

Comparisons of the effect of the air volume fraction on the velocity distributions obtained by the SPIV technique

at three axial positions of $Z= -395$ mm, -75 mm and 295 mm for varied air volume fraction between 18% and 25.42% are shown in Figures 4-8. All experimental measurements at $Z= -395$ mm and -75 mm presented in this paper were extracted along the $Y=0$ line. However, it was not possible to extract enough data for graphical interpretation at $Z= 295$ mm along the $Y=0$ section due to the conventional SPIV processing algorithm used in this investigation (as discussed in SPIV set-up) that cannot differentiate between the velocity distributions of each phase present in the multiphase flow. In addition, as air separates from the mixture and then concentrates at the upper section of the pipe separator it introduces shadows that hampers visibility. This reduces the amount of information present in the PIV images. Therefore, contour plot of the velocity profiles are then presented at $Z= 295$ mm axial position.

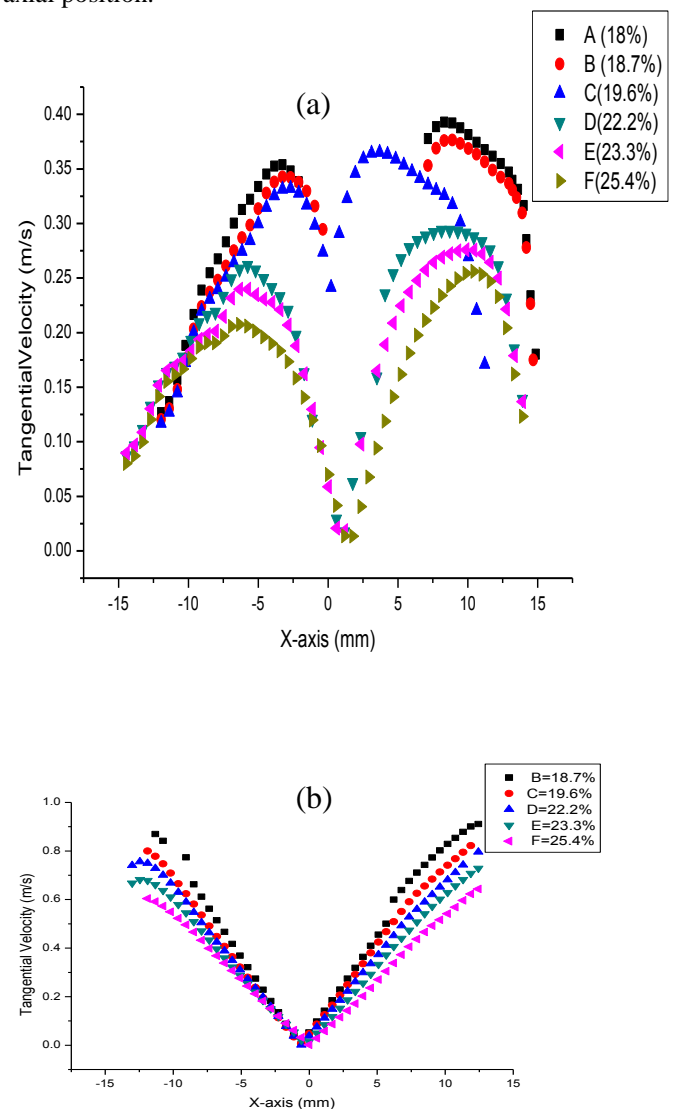


Figure 4: Effect of Air Volume Fraction on the Averaged Tangential Velocity of Water-Air Flow at Axial Positions of (a) $Z=-395$ mm (b) $Z=-75$ mm.

Figure 4(a-b) shows the tangential velocity of the air-water flow at the $Z=-395$ mm and -75 mm axial positions increases away from the centre of the tube, reaching a

maximum and then decreases close to the wall. The magnitudes of the tangential velocity increases at any x-axis coordinate as the air volume fraction decreases. The results show that an increase in air volume fraction does not affect the tangential velocity flow pattern in a pipe separator. However, similar tangential velocity profile was reported in previous works on cyclones with similar shapes to the one in this study [21- 23].

increase in the air volume fractions. However, at negative values of the x-axis, axial velocity increases with air volume fraction.

Figure 5(b) shows that the magnitude of the axial velocity profiles increases with air volume fraction away from the centre of the tube. However, close to the wall at positive x-axis coordinates the magnitude of the axial velocity profiles increases with the volume fraction of air. Therefore, we can conclude that air volume fraction is inversely related to the inlet flow rate of the air-water mixture. The results show that the magnitude of the axial velocity profile is a function of the inlet flow rate. The measured axial velocity pattern is consistent with literature reports [23-24].

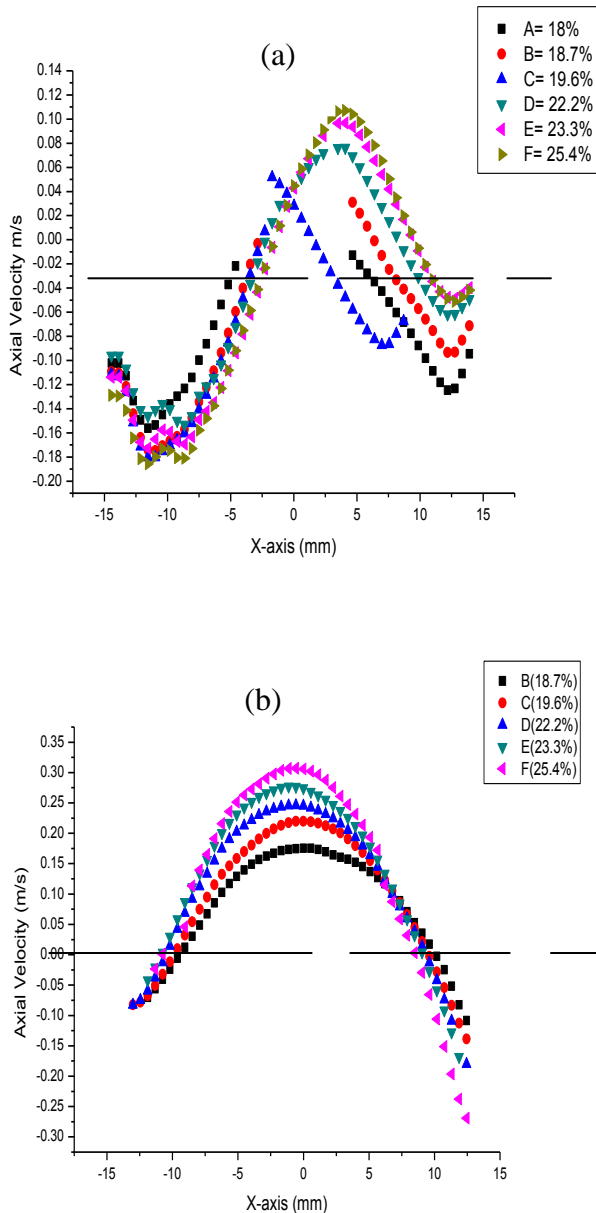


Figure 5: Effect of Air Volume Fraction on the Averaged Axial Velocity of Water-Air Flow at Axial Position of (a) Z=-395 mm (b) Z=-75 mm.

Figure 5(a-b), shows the effect of air volume fractions on the mean axial velocity at the three axial positions. The axial velocity profiles show an upward flow region at the centre of the tube and a downward flow region at the wall. These profiles, however, do have similar shapes. That is, a difference in air volume fraction does not affect the axial velocity flow pattern. Figure 5(a) shows that the magnitude of the axial velocity profiles increases with an increase in air volume fractions in the upward flow region. At positive values of the x-axis, axial velocity decreases with an

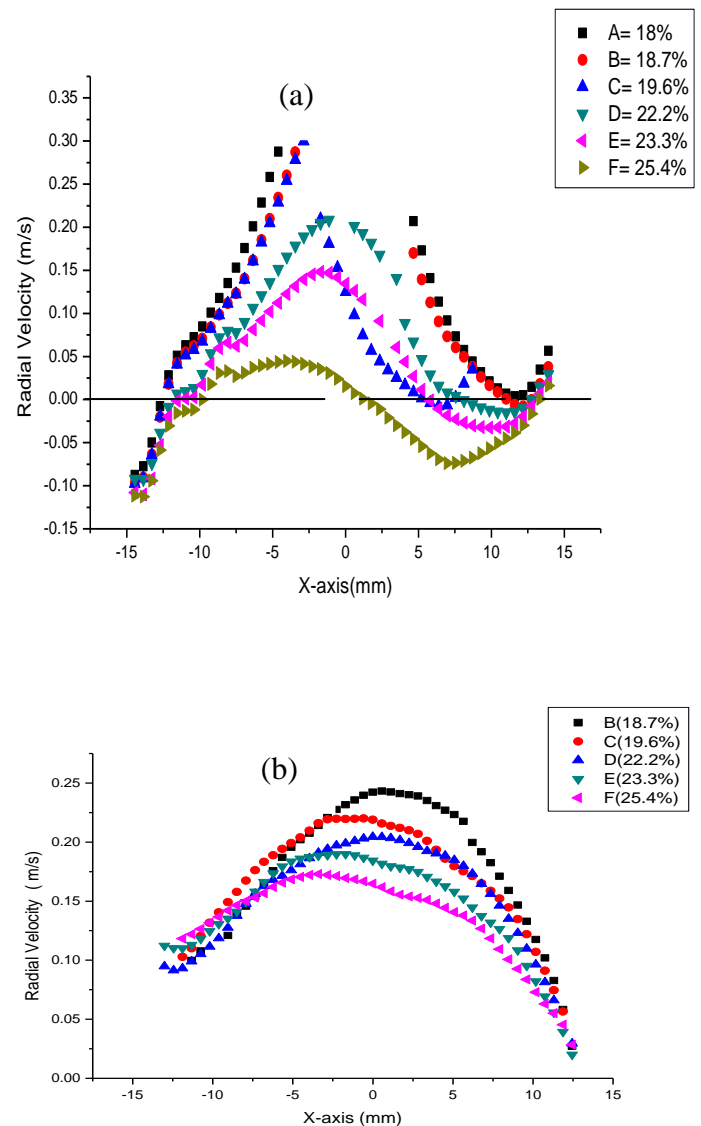


Figure 6: Effect of Air Volume Fraction on the Averaged Radial Velocity of Water-Air flow at Axial Positions of (a) Z=-395 mm (b) Z=-75 mm.

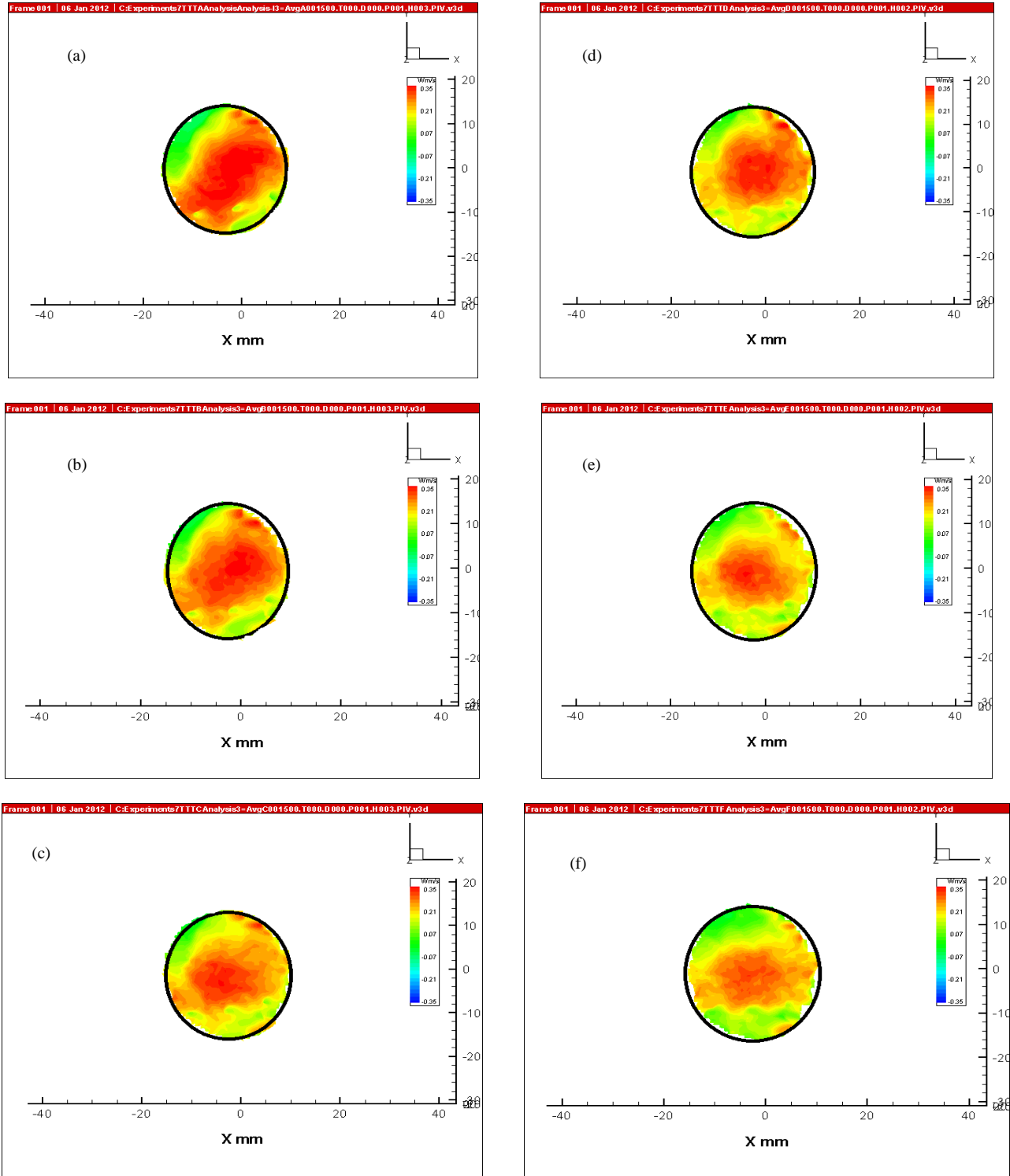


Figure 7: Contour Plots of the Mean Axial Velocity for Water flow and Air-Water flow at Z = 295 mm axial position.

- (a): $2.05 \times 10^{-4} \text{ m}^3/\text{s}$ (water), $4.5 \times 10^{-5} \text{ m}^3/\text{s}$ (air); (b): $1.96 \times 10^{-4} \text{ m}^3/\text{s}$ (water), $4.5 \times 10^{-5} \text{ m}^3/\text{s}$ (air); (c): $1.85 \times 10^{-4} \text{ m}^3/\text{s}$ (water), $4.5 \times 10^{-5} \text{ m}^3/\text{s}$ (air);
 (d): $1.58 \times 10^{-4} \text{ m}^3/\text{s}$ (water), $4.5 \times 10^{-5} \text{ m}^3/\text{s}$ (air); (e): $1.48 \times 10^{-4} \text{ m}^3/\text{s}$ (water), $4.5 \times 10^{-5} \text{ m}^3/\text{s}$ (air); (f): $1.32 \times 10^{-4} \text{ m}^3/\text{s}$ (water), $4.5 \times 10^{-5} \text{ m}^3/\text{s}$ (air);

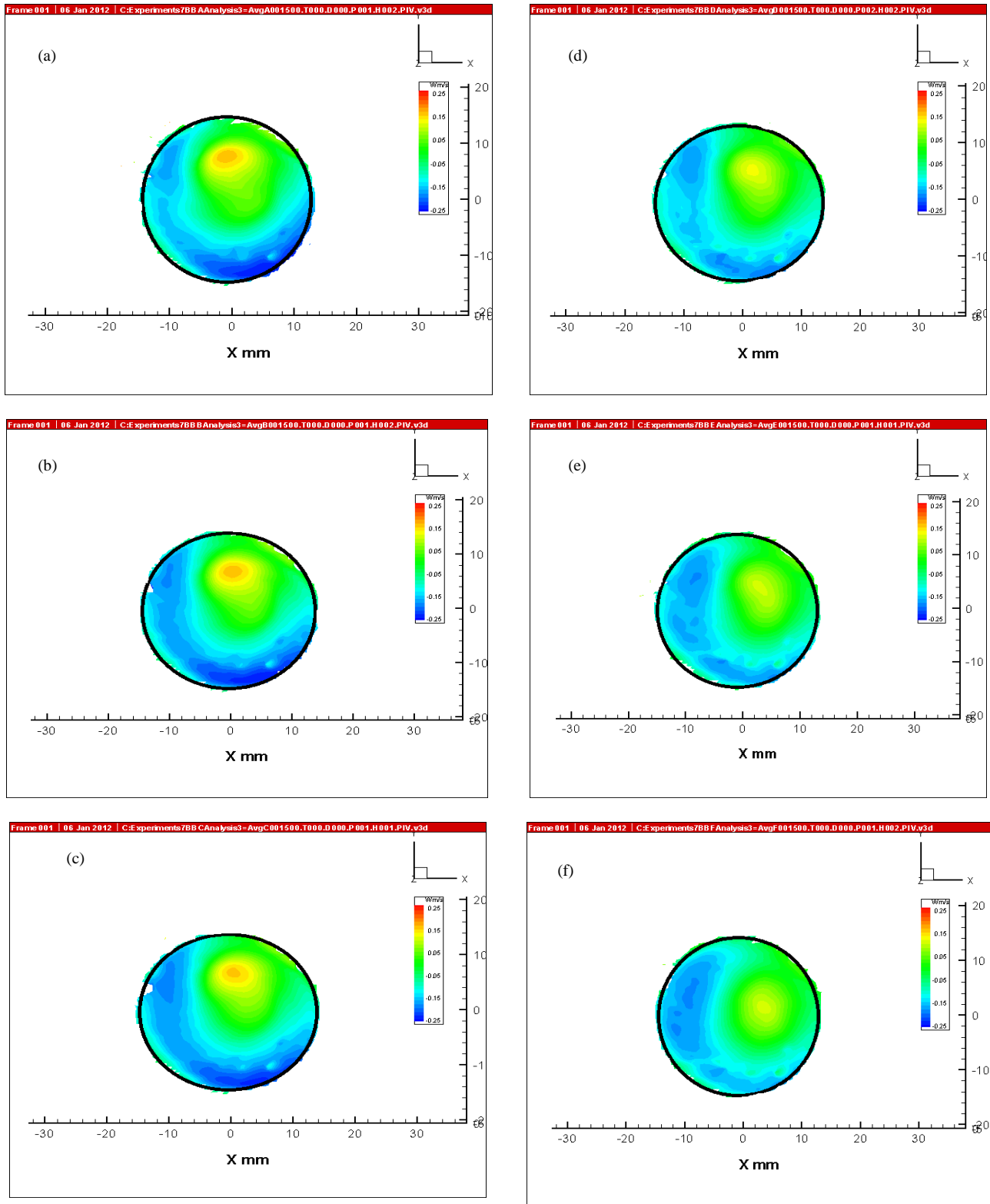


Figure 7: Contour Plots of the Mean Axial Velocity for Water flow and Air-Water flow at $Z = -395$ mm axial position.

(a): $2.05 \times 10^{-4} \text{ m}^3/\text{s}$ (water), $4.5 \times 10^{-5} \text{ m}^3/\text{s}$ (air); (b): $1.96 \times 10^{-4} \text{ m}^3/\text{s}$ (water), $4.5 \times 10^{-5} \text{ m}^3/\text{s}$ (air); (c): $1.85 \times 10^{-4} \text{ m}^3/\text{s}$ (water), $4.5 \times 10^{-5} \text{ m}^3/\text{s}$ (air);
 (d): $1.58 \times 10^{-4} \text{ m}^3/\text{s}$ (water), $4.5 \times 10^{-5} \text{ m}^3/\text{s}$ (air); (e): $1.48 \times 10^{-4} \text{ m}^3/\text{s}$ (water), $4.5 \times 10^{-5} \text{ m}^3/\text{s}$ (air); (f): $1.32 \times 10^{-4} \text{ m}^3/\text{s}$ (water), $4.5 \times 10^{-5} \text{ m}^3/\text{s}$ (air)

Figures 6(a-b) shows the mean radial velocity field plotted as a function of air volume fraction. As shown in Figure 6(a), the magnitude of radial velocity decreases with an increase in the air volume fraction at all x-axis coordinates. In Figure 6(b) the magnitude of radial velocity profiles decreases with an increase in the air volume fraction at the centre of tube and at positive x-axis coordinates. The shapes of the radial velocity profiles are observed to be unaffected by different air volume fractions at the inlet. Therefore, we can conclude that, radial profiles are essentially independent of the air volume fraction at the inlet.

An increased in the air volume fraction is observed in Figure 7 to be associated with more surface area in the contour plots of the axial velocity of air-water flow occupied by the upward flow. It means that as the volume fraction of air increases, the concentration of air flow in the air-water flow field increases with most of the air flow in the air-water mixture separates and moves upward to flow out through the gas outlet of the pipe separator. This study is helpful in understanding the phase separation that occurred as air-water flow through the pipe separator. Figure 8 shows an increase in the magnitude of the axial velocity as air volume decreases. However, the axial velocity pattern is unaffected by changes in the air volume fraction of the inlet mixture. Therefore, an increased in the air volume fraction is accompanied by more air concentrating at $Z=295$ mm and promotes a higher separation efficiency for air-water mixture flowing through the pipe separator.

IV. CONCLUSION

By using a Stereo-PIV technique, the effect of air volume fraction on the tangential velocity, axial velocity and radial velocity at different axial positions were determined in 30 mm pipe separator. The results are summarized as follows:

(a) The magnitudes of the tangential and radial velocities are function of the air volume fraction at the inlet and the flow profiles are not affected by changes in the air volume fraction.

(b) At $Z= -75$ mm and -395 mm, the axial velocity flow pattern is unaffected by changes in the air volume fraction. However, the magnitude of axial velocity at these axial positions increases with a decrease in air volume fraction.

(c) The axial velocity flow pattern at $Z= 295$ mm is affected by changes in the air volume fraction. An increased in the air volume fraction resulted in more surface area in the contour plot being occupied by air that separate from the air-water mixture. This show that an increase in air volume fraction leads to higher separation efficiency for air-water mixture flowing through the pipe separator.

ACKNOWLEDGEMENT

Authors thankfully acknowledge EPSRC and TSI Inc for the useful support and discussions relevant to this work. The authors acknowledge funding from the Petroleum Technology and Development Fund (PTDF), Nigeria.

NOMENCLATURE

d	Pipe diameter (m)
U_G	Gas superficial velocity (ms^{-1})
U_L	Liquid superficial velocity (ms^{-1})
ρ_G	Gas phase density (Kgm^{-3})
ρ_L	Liquid phase density (Kgm^{-3})
μ_L	Liquid phase viscosity (Pa.s)
$(\Delta P/L)$	Frictional pressure drop (Pa m^{-1})

REFERENCES

1. Raffel, M., Willert, C. and Kompenhans, J. Particle Image Velocimetry: A Practical Approach. (Springer London 2007).
2. Adrian R. J. Twenty years of particle image velocimetry. *Experiments in fluids*, 39:2 (2005) 159-169.
3. Westerweel, J. (1997) 'Fundamentals of digital particle image velocimetry', *Measurement Science and Technology*, 8:12 (1997) pp. 1379-1392.
4. Prasad, A. K. Stereoscopic Particle Image Velocimetry, *Experiments in Fluids*, 29, (2000) pp. 103-116.
5. Adrian, R. J. and Westerweel, J. *Particle Image Velocimetry* Cambridge University Press London 2011.
6. Li, Ya-lin ; Yuan, Shou-qi ; Tang, Yue ; Yuan, Jian-ping, Motion of Tracer Particles in a Centrifugal Pump and its Tracking Characteristics, *Journal of Hydrodynamics, Ser.B, , Vol.24.5, (2012) pp.785-793.*
7. Ragnid, S.F and Van Oudheusden, B.W; Particle tracer response across shock measured by PIV. *Experiments in fluids*, 50:1 (2011) pp. 53-64.
8. Liu, Z., Jiao, J., Zheng, Y., Zhang, Q. and Jia, L. Investigation of turbulence characteristics in a gas cyclone by stereoscopic PIV', *AIChE Journal*, 52, (12) (2006) pp. 4150-4160.
9. Bellani, G. Experimental Studies of Complex flow through Image-based Techniques. Royal Institute of Technology KTH, (2011) Stockholm, Sweden.
10. Ng,I. Paganin, D.M and Fouras, A; Optimization of in-line phase contrast particle image velocimetry using a laboratory x-ray source , *Journal of Applied Physics* 112, (2012) 074701
11. Hassan, Y. A. 'Multiphase Bubbly Flow Visualization Using Particle Image Velocimetry', Annual New York Academy of Sciences, (2002) 972.
12. Hassan, Y. A., Schmidl, W.D and Ortiz- Villafuerte, J. 'Three Dimensional Bubbly Flow Measurement Using PIV, *Journal of Visualization*, 1, 3 (1999) pp. 291 - 301.
13. Vestøl, S. and Melaaen, M.C. Velocity profile measurements on stratified two-phase gas/liquid flow in horizontal and downwardly inclined pipes using PIV, "5th international conference on heat transfer, fluid mechanics and thermodynamics, HEFAT 2007", Sun City, South Africa, 1-4 July, 2007.
14. Liu, Hai-fei, Xu, Jing-yu and Zheng, Zhi-chu; Numerical study on oil and water two-phase flow in a cylindrical cyclone, *Journal of hydrodynamics* 22:5 (2010) pp: 832-837.
15. Vazquez, C. O. *Multiphase flow separation in Liquid-Liquid cylindrical cyclone and Gas-Liquid -Liquid cylindrical cyclone compact separators* PhD dissertation, The University of Tulsa, USA 2001.
16. Afolabi, E.A, *Experimental Investigation and CFD Simulation of Multiphase flow in a Three Phase Pipe Separator.* Ph.D dissertation. School of Chemical Engineering and Advanced Materials, Newcastle University, Newcastle, UK 2012.
17. Afolabi, E.A and Lee, J.G.M, " Stereoscopic particle image velocimetry analysis of air-water flow in a pipe separator" International Reveiw of Chemical Engineering,, Rapid Communication, in press.
18. Reyes-Gutiérrez, M. A., Rojas-Solórzano, L. R., Colmenares, J., Marín-Moreno, J. C. and Meléndez-Ramírez, A. J. 'Eulerian-

- Eulerian modeling of disperse two- phase flow in a gas-liquid cylindrical cyclone., *Journal of Fluids Engineering, Transactions of the ASME*, 125, (2006) pp. 832- 838.
19. Barnea, D. A unified model for predicting flow-pattern transitions for the whole range of pipe inclinations, *International Journal of Multiphase Flow*, 13, 1 (1986) pp. 1-12.
 20. Perez, Valente Hernandez; *Gas-liquid two-phase flow in inclined pipes* Ph.D dissertation, The University of Nottingham 2007.
 21. Bergström, J. and Vomhoff, H. Experimental hydrocyclone flow field studies, *Separation and Purification Technology*, 53, 1 (2007) pp. 8-20.
 22. Concha, F. Flow Pattern in Hydrocyclones', *Kona-Powder and Particle*, 25, (2007) pp. 97-132.
 23. Siangsanun, V., Guigui, C., Morchain, J., Marteil, P., Levecq, C., Puprasert, C. and Hébrard, G. Velocity measurement in the hydrocyclone by oil droplet, doppler ultrasound velocimetry, and CFD modelling, *Canadian Journal of Chemical Engineering*, 89:4 (2011) pp. 725-733.
 24. Bai, Z. S., Wang, H. I. and Tu, S. T. Experimental study of flow patterns in deoiling hydrocyclone, *Minerals Engineering*, 22, 4 (2009) pp. 319-323.